PERGAMON

International Journal of Solids and Structures 39 (2002) 4249–4269

INTERNATIONAL JOURNAL OF SOLIDS and STRUCTURES

www.elsevier.com/locate/ijsolstr

Analysis of the dynamic propagation of adiabatic shear bands

A.-S. Bonnet-Lebouvier [1], A. Molinari *, P. Lipinski [2]

Laboratoire de Physique et Mécanique des Matériaux, U.M.R. CNRS 7554, ISGMP, Ecole Nat. d'Ingenieurs de Metz, Université de Metz, Ile du Saulcy, 57045 Metz Cedex 01, France

Received 24 July 2001; received in revised form 5 March 2002

Abstract

The dynamic propagation of adiabatic shear bands is analysed. In the numerical simulations, a layer of finite length and finite thickness is subjected to shear loading. After a transient, a steady state is attained in which adiabatic shear bands propagate with a constant velocity. The evolution of the shear band speed is determined as a function of the applied velocity. A dimensional analysis allows to determine a general law describing the influence of each problem's parameter on the shear band speed. The effects of heat conduction are discussed in details. Finally the concept of a process zone is introduced. The process zone is a region propagating with the shear band tip, where an intense stress softening is produced by thermo-mechanical coupling. It is shown how the shear band propagation is controlled by this stress softening.

Keywords: Adiabatic shear band; Shear band speed; Thermal softening; Process zone

1. Introduction

Adiabatic shear banding has been widely studied during the last decades as it is a phenomenon frequently encountered in materials submitted to high strain rates. The mechanism of formation of these bands as a result of thermo-mechanical instability has been analysed in detail by many authors, e.g. Clifton (1980), Bai (1982), Merzer (1982), Wright and Batra (1985), Molinari and Clifton (1987), Giovanola (1988a,b) and Molinari (1988), but the phenomenon of propagation is less known.

Among the recent studies carried out on this subject, the work of Marchand and Duffy (1988) enabled to evaluate the speed of propagation of a shear band in a thin-walled HY 100 steel tube twisted at a strain rate of 1600 s^{-1}. The speed of propagation was estimated to be 520 m/s in the case where only one tip of the

* Corresponding author. Tel.: +33-3-87-31-53-69; fax: +33-3-87-31-53-66.

E-mail addresses: asbonnet@lpmm.univ-metz.fr (A.-S. Bonnet-Lebouvier), molinari@lpmm.univ-metz.fr (A. Molinari), lipinski@lpmm.univ-metz.fr (P. Lipinski).

[1] Tel.: +33-3-87-31-53-81.

[2] Tel.: +33-3-87-31-54-01.

0020-7683/02/$ - see front matter
PII: S0020-7683(02)00244-5

band propagates and 260 m/s in the case of a two-directional propagation. Kalthoff and Wrinkler (1987) studied double-notched plates impacted with a cylindrical projectile. They reported a transition of the failure mode between crack propagation and adiabatic shear band propagation depending on the notch-tip radius and the impact velocity. Grady (1992) considered a simple model of propagating shear bands, based on results of a one-dimensional analysis. Batra and Zhang (1994) reproduced numerically the experiments of Marchand and Duffy for three different values of strain rates: 1000, 5000 and 25 000 s^{-1}. They obtained a shear band propagating in both directions along the tube circumference and with a non-stationary speed varying, for example for a strain rate of 1000 s^{-1}, from 40 to 260 m/s. They also found a strong dependence of the speed of propagation on the nominal strain rate. Gioia and Ortiz (1996) used a boundary layer theory to study the two-dimensional structure of a shear band propagating in a thermo-viscoplastic solid. Zhou et al. (1996a) used impacted prenotched plates to study numerically and experimentally the propagation of an adiabatic shear band in C300 steel. A strong dependence of shear band speed on impact velocity, at lower impact velocities, and a tendency to saturate at higher impact velocities were observed. More recently, Mercier and Molinari (1998) developed an analytical model to determine the speed of propagation of an adiabatic shear band propagating into an infinite layer of finite thickness submitted to shear loading. The influence of strain hardening, strain-rate sensitivity, thermal softening and elastic shear modulus was characterized on the shear band speed and on the length of the process zone. Heat conduction was neglected. With this model and for a CRS 1018 steel, the shear band velocity reported was about 1200 m/s.

In this paper, the propagation of an adiabatic shear band is modelled by numerical simulations. A layer of finite length and finite thickness is submitted to simple shear. Heat conduction is taken into account. After a transient, a steady state is attained in which the band propagates with a constant velocity.

The paper is organized as follows. Firstly, the model and the constitutive equations are presented. Then, the results giving the evolution of the shear band speed as a function of the applied velocity are shown. A comparison is made between the case where heat conduction is taken into account and the adiabatic case. The width of the shear band is evaluated. In the followings of the paper, a dimensional analysis allows to determine a general law describing the influence of each problem's parameter on the shear band speed. Finally our attention is focussed on the process zone, which is defined as the region near the shear band tip where the essential part of the localization process occurs. It is shown that shear band propagation is driven by the stress softening produced within the process zone.

2. Modelling

We assume the material to be elastic thermo-viscoplastic. The elastic law takes the following form:

$$\sigma^*_{ij} = C_{ijkl} d^{\mathrm{e}}_{kl} \tag{1}$$

where C_{ijkl} are the elastic moduli and d^{e}_{kl} is the elastic strain rate. The total strain rate d is the sum of the plastic strain rate d^{p} and the elastic strain rate d^{e}.

$$d = d^{\mathrm{p}} + d^{\mathrm{e}} \tag{2}$$

In (1), $\sigma^*_{ij} = \dot{\sigma}_{ij} - \omega_{jk}\sigma_{ki} - \omega_{ik}\sigma_{kj}$ denotes the Jaumann rate of the stress tensor, with ω_{jk} being the anti-symmetric part of the velocity gradient.

Two distinct constitutive laws are studied to govern the plastic part of the deformation. The first one from Molinari and Clifton [6]:

$$\sigma_{\mathrm{e}} = K(\bar{\varepsilon}^{\mathrm{p}} + \varepsilon^{\mathrm{p}}_0)^n T^{-\nu} (D^{\mathrm{p}}_{\mathrm{eq}} + D^{\mathrm{p}}_0)^m \tag{3}$$

Table 1
Material parameters of CRS 1018 steel

Parameter	CRS 1018
K	6300×10^6 Pa
m	0.019
n	0.015
v	0.38
C_p	500 J/kg K
k	50 W/m K
ρ	7800 kg m^{-3}
$\varepsilon_0^{\mathrm{p}}$	0.057
D_0^{p}	10^{-3}
μ	80 GPa

where σ_{e} and $D_{\mathrm{eq}}^{\mathrm{p}}$ represent the effective stress and the effective plastic strain rate, respectively given by

$$\sigma_{\mathrm{e}} = \left(\frac{3}{2} s_{ij} s_{ij}\right)^{1/2}, \qquad D_{\mathrm{eq}}^{\mathrm{p}} = \left(\frac{2}{3} d_{ij}^{\mathrm{p}} d_{ij}^{\mathrm{p}}\right)^{1/2} \tag{4}$$

s_{ij} corresponds to the deviatoric stress tensor and d_{ij}^{p} is given by the J_2 flow theory:

$$d_{ij}^{\mathrm{p}} = \frac{3}{2} \frac{D_{\mathrm{eq}}^{\mathrm{p}}}{\sigma_{\mathrm{e}}} s_{ij} \tag{5}$$

The cumulated plastic strain is defined by:

$$\bar{\varepsilon}^{\mathrm{p}}(t) = \int_0^t D_{\mathrm{eq}}^{\mathrm{p}}(t')\,\mathrm{d}t' \tag{6}$$

The flow stress level is scaled by K, $\varepsilon_0^{\mathrm{p}}$ is a plastic prestrain, n is the strain hardening exponent ($n > 0$), T is the absolute temperature, v ($v > 0$) and m ($m > 0$) are respectively the thermal softening and the strain rate sensitivity exponents.

The values of this constitutive law's parameters are reported in Table 1 for a CRS 1018 steel. These values were found in Clifton et al. (1984) for nominal strain rates varying from 700 to 1200 s^{-1}. For high temperatures the constitutive law (3) becomes unadapted as the stress drops to only half its initial value when the melting temperature is reached.

As a consequence the second constitutive law is introduced, which keeps the same structure as (3) but where the stress drops to zero when the melting temperature is reached:

$$\sigma_{\mathrm{e}} = K'(\bar{\varepsilon}^{\mathrm{p}} + \varepsilon_0^{\mathrm{p}})^n (D_{\mathrm{eq}}^{\mathrm{p}} + D_0^{\mathrm{p}})^m \left(1 - \left(\frac{T - T_0}{T_m - T_0}\right)^p\right) \tag{7}$$

T_0 and T_{m} are the initial and melting temperatures respectively ($T_0 = 300$ K and $T_{\mathrm{m}} = 1800$ K), K' corresponds to KT_0^{-v} and p adjusts the rate of the stress drop. The value of p ($= 0.85$) is chosen to make (3) and (7) as close as possible for temperatures included between 300 and 500 K and for a strain rate $\dot{\gamma} = 1000$ s^{-1}, see Fig. 1.

The comparison between those two constitutive laws will be carried out in order to see the influence of the stress drop on the shear band propagation.

At high strain rates ($\geqslant 10^3$–10^4 s^{-1} for steels), a strong increase of the strain rate sensitivity is observed. This phenomenon is not accounted for by the laws (3) and (7). However, by changing the value of m in these laws, the influence of the strain rate sensitivity on shear band propagation will be analysed.

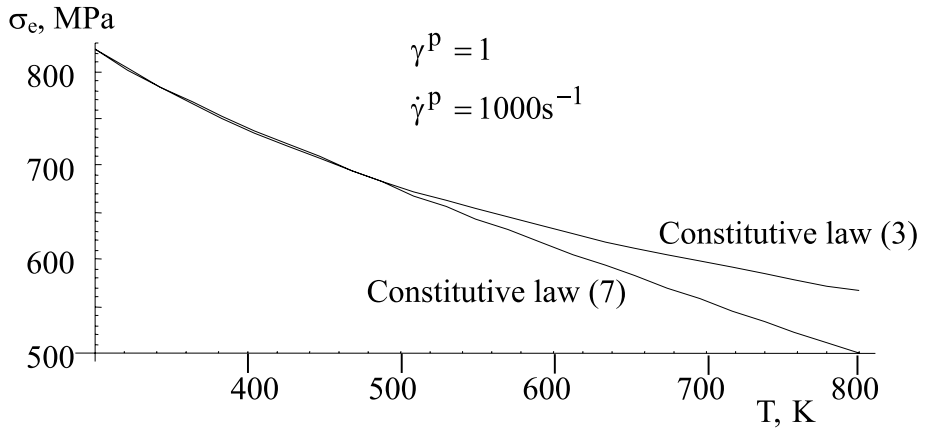

Fig. 1. Evolution of the effective stress σ_e in terms of temperature for $\gamma^p = 1$, $\dot{\gamma}^p = 1000\ s^{-1}$ and for two different hardening laws (3) and (7). For the constitutive law (7), the parameter p equals 0.85. Note that, for these two laws, the thermal softening is identical when $300 \leqslant T \leqslant 500$ K, but differs significantly for larger temperatures.

Considering our problem as two-dimensional, the energy equation providing the evolution law for the temperature has the form:

$$\rho C_p \dot{T} - k\left(\frac{\partial^2 T}{\partial x^2} + \frac{\partial^2 T}{\partial y^2}\right) = \beta \sigma_e \dot{\bar{\varepsilon}}^p \tag{8}$$

where C_p is the heat capacity, ρ is the mass density, k is the heat conductivity and β is the Taylor–Quinney coefficient which defines the fraction of plastic work converted into heat; usually β is taken constant and equal to 0.9.

We consider a specimen of finite length L with uniform properties and uniform height $2h$, Fig. 2. A frame Oxy is defined, with Ox being the shear direction. Constant velocities $v_x = \pm V$ and $v_y = 0$ are prescribed at the boundaries $y = +h$ and $y = -h$ respectively. Displacements of the boundary $x = 0$ are imposed to be equal to those of the boundary $x = L$, in order to better approach the tubular specimen used in Marchand and Duffy's experiments. The shear layer considered here can be viewed as the wall of the tube developed in a plane, with the difference that we consider here plane strain conditions, all quantities being independent of z. The total length of the layer is 200 mm and the width $2h$ is equal to 2.5 mm, see Fig. 2. A geometrical defect is introduced on a small part of the specimen by imposing a reduction of thickness of 20% on a rectangular domain (≈60 μm in y-direction and ≈200 μm in x-direction). The magnitude of this defect plays

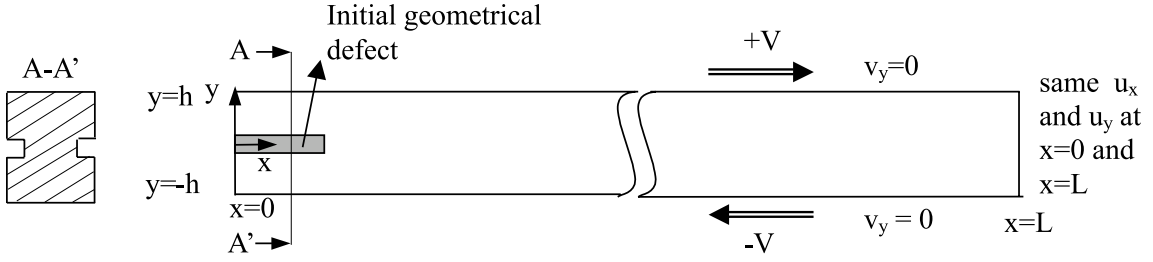

Fig. 2. Schematic view of a finite layer of steel, length $L = 200$ mm, width $2h = 2.5$ mm. Constant velocities $v_x = \pm V$ and $v_y = 0$ are applied at the boundaries $y = \pm h$. Periodic boundary conditions are taken at the extremities $x = 0$ and $x = L$. An initial geometrical defect is introduced (thickness $e_{def} < e$, length ≈200 μm, width ≈60 μm).

a role on the time to localization but has no effect on the stationary shear band speed. We chose a high defect amplitude to spare some calculation time. This zone of lower thickness is situated in the middle of the specimen at the left boundary. Adiabatic thermal conditions are assumed on the specimen boundaries.

The initial velocity field is supposed to vary linearly from $v_x = -V$ on the boundary $y = -h$ to $v_x = +V$ on the boundary $y = h$. These conditions correspond to the velocity field existing in Marchand and Duffy's specimen (1988) when the adiabatic shear band initiates.

Numerical analyses are performed with the FE ABAQUS/Explicit code (2000). A two-dimensional finite element model is applied. The available 'plane strain' 2D elements CPE4RT are used.

3. Influence of loading conditions and of material and geometrical parameters

Nominal strain rates varying from $\dot{\gamma} = 400$ to 2.4×10^5 s^{-1} are considered. They correspond to applied velocities V in the range from 0.5 to 300 m/s as $\dot{\gamma} = V/h$. After a transient, a steady state is attained in which two shear bands emanating from the boundaries $x = 0$ and $x = L$ propagate with a constant velocity. The presence of those two bands is due to the periodicity on the boundary conditions imposed at these extremities. It is of note that in this problem, the shear band width is structured by heat conductivity. Therefore the results obtained are mesh independent as the width of the shear band is physically determined.

3.1. Velocity profiles

In the region situated far ahead the band, the velocity profile is linear on v_x (and $v_y = 0$) while in the region situated behind the shear band tip and on each side of the adiabatic shear band, we have rigid body motions with velocities $v_x = \pm V$ (Fig. 3).

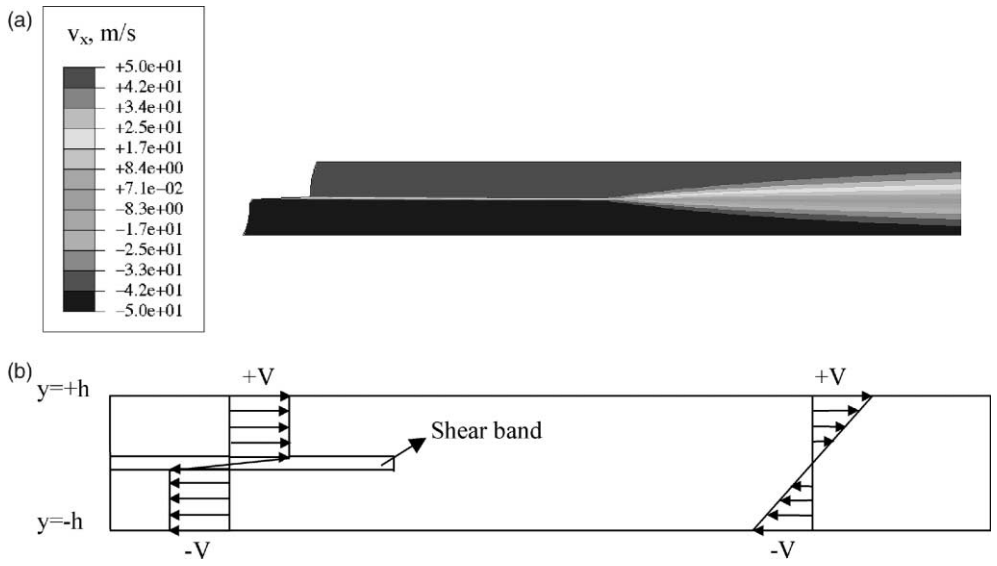

Fig. 3. (a) View of the component v_x of the velocity profile for a nominal strain rate of 4×10^4 s^{-1}. The region situated far ahead the shear band tip is submitted to a linear velocity profile while the regions situated behind the shear band tip are submitted to rigid body motions. (b) Schematic view of the transition between the two v_x velocity profiles.

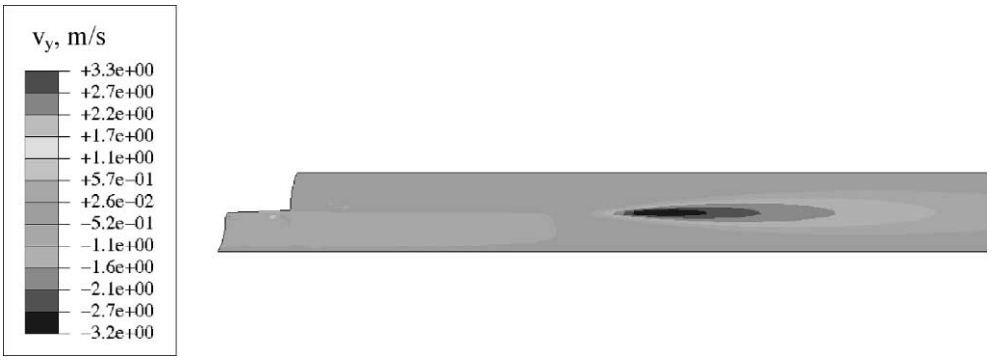

Fig. 4. View of the velocity component v_y at the tip of the shear band for a nominal strain rate of 4×10^4 s^{-1}. The negative values of v_y indicate a flow of material from the upper part of the specimen to the lower part.

Along the y-direction, the velocity field v_y presents negative values at the tip of the shear band (Fig. 4). These negative values indicate a material transfer from the upper to the lower part of the specimen, phenomenon already reported by Mercier and Molinari (1998) in their two-dimensional analytical model. This material flow is necessary to get a band propagation in a layer of finite thickness subjected to the boundary conditions specified on the Fig. 2.

3.2. Dependence of the shear band speed upon the applied velocity (stationary conditions)

The influence of the applied velocity V on the shear band propagation speed C is illustrated in Fig. 5. To evaluate C, strain isolines are followed with time. Both constitutive laws give the same results. This point will be discussed later.

Three stages are visible according to Fig. 5. A zoom of the C versus V curve for low velocities reveals the existence of a threshold V_c for the applied velocity below which no shear band propagation is obtained. This minimum value was already reported by Zhou et al. (1996a,b) for impacted prenotched plates of C300 steel (see Fig. 11 of Zhou et al., 1996b). As the width of the specimen is fixed, the minimum velocity corresponds to a minimum strain rate. The existence of this minimum strain rate for localization was already predicted by Wright and Walter (1987).

In stage I, the variation of C upon V is almost linear. Stage II shows a tendency towards an asymptotic value and finally, in stage III, a very slight evolution of C is observed with V. Although Zhou et al. (1996a,b) could not reach any stationary process in their numerical work, they revealed, using an average shear band speed, the presence of stages I and II but could not characterize the stage III because of a lack of data at very high strain rates.

3.3. Evolution of the shear band width w as a function of the applied velocity V

To capture the dependence of the shear band width with respect to V, a great attention must be given to the mesh used for the calculations, as the size of the shear band width can be very small (<10 μm). To find an acceptable compromise between the quality of the solution and the calculation time, several meshes are considered. The length of the modelled specimen must be large enough to allow the shear band to reach a stationary process and to prevent the strong interaction between the two bands emanating from the left and right edges. Moreover, the localization process must take place on several elements to avoid mesh dependence. As a wide range of nominal strain rates is considered and as the width of the shear band is directly dependent on this strain rate, the meshes represented in Fig. 6 are used. The first one (a) is used for

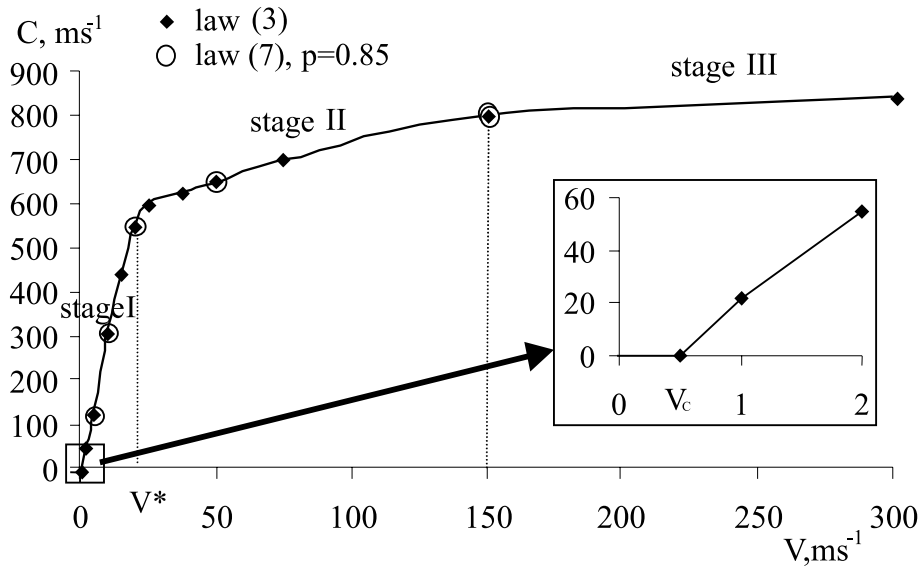

Fig. 5. Effects of the applied velocity V on the stationary shear band speed C. A CRS 1018 steel is considered and two different constitutive laws (3) and (7) are used. The enlarged box shows the existence of a critical velocity V_c below which no propagation is observed due to heat conductivity effects: transition from isothermal ($V \ll V_c$) to adiabatic process ($V \gg V_c$). Note the presence of three stages. In stage I ($V < V^*$), the band propagation is controlled by external work. In stage III, the propagation is driven by the elastic energy release.

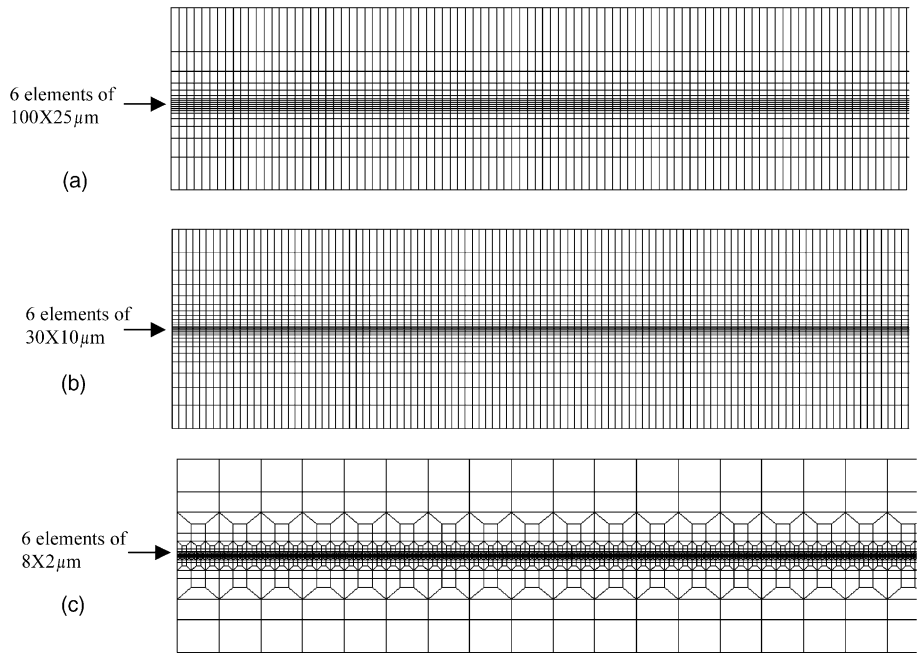

Fig. 6. Meshes used for the calculations. a: for $V < 5$ m/s, b: for $5 \leqslant V < 50$ m/s, c: for $V \geqslant 50$ m/s.

applied velocities $V < 5$ m/s and includes six 25-μm width central elements with a regular progression along the y-direction. The second one (b) is used for $5 \leqslant V < 50$ m/s and the central elements are 10-μm width. The last one (c) is used for applied velocities $V \geqslant 50$ m/s. This mesh has six 2-μm width central elements but shows a rapid evolution of the element size when leaving the shear band zone to spare some calculation time.

The dependence of the shear band width w upon V is illustrated in Fig. 7 for constitutive laws (3) and (7); w characterizes the width of the zone having a strain rate bigger than 1/10 of the maximum strain rate. The size of the shear band is measured far behind the shear band tip. An increase of V leads to a reduction of w as the produced heat has less time to diffuse in the specimen. According to Fig. 7, the following relationships are obtained for w:

$$w = aV^{-0.5} \tag{9}$$

for constitutive law (3) and

$$w = bV^{-0.96} \approx bV^{-1} \tag{10}$$

for constitutive law (7). Because of the low values of w obtained for constitutive law (7) a finer mesh should be used for high values of V.

Wright and Ockendon (1992) and Dinzart and Molinari (1998) obtained an expression similar to (10) in their one-dimensional quasi-static analysis of a fully formed shear band. Using a constitutive law in which the stress drops linearly when the temperature increases, they found that the shear band width was inversely proportional to the velocity applied on the specimen. As in constitutive law (7), the stress drop due to thermal softening is almost linear for $p = 0.85$, it can be observed that the results obtained by these authors are comparable to those reported here.

As a conclusion, the width of the shear band is directly linked to the type of constitutive law considered. Wright and Ravichandran (1997) already obtained asymptotic results for fairly general flow laws including an error criterion used in evaluating its applicability to several common flow rules. Interesting results on the structure of a fully developed band were also given by Glimm et al. (1993). However it is possible to compare the values of w obtained in our simulations with those reported by the experimental tests of Marchand and Duffy (1988) on a CRS 1018 steel. They measured for a nominal strain rate of 1600 s^{-1} (i.e. for an applied velocity $V = 2$ m/s) shear band widths of the order of 100 μm. For this value of strain rate,

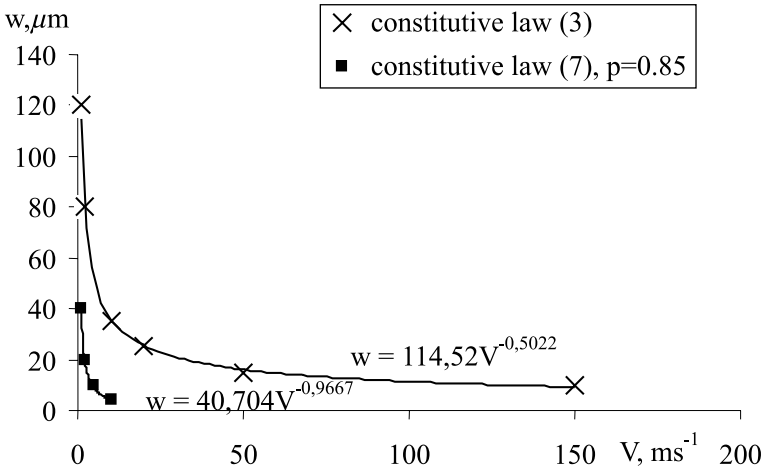

Fig. 7. Evolution of the shear band width w as a function of the applied velocity V for two different constitutive laws (3) and (7).

the values of w reported in our simulations are respectively 80 μm for constitutive law (3) and 20 μm for constitutive law (7).

3.4. Comparison with the adiabatic case

To analyse the effects of heat conduction on the shear band propagation, the dependence of the shear band speed upon the applied velocity is analysed here by neglecting heat conductivity (adiabatic conditions). As the results obtained in the case including heat conduction were the same for both constitutive laws (3) and (7), adiabatic calculations are carried out only for the law (3). In the adiabatic framework, the shear band width w is no more defined because of the absence of heat diffusion. Then, the localization of deformation appears to be concentrated on a single element which determines artificially the width of the shear band.

If we attribute to this central element a width w_{el} identical to the shear band width calculated in the full problem including heat conduction, the results shown in Fig. 8 are obtained. These results are very close for both configurations (adiabatic and heat conducting cases), excepted for low values of V. For $V < V_c$, no shear band propagation is observed in the calculations including heat conductivity. Consequently, an arbitrary value is introduced for w_{el} in the adiabatic configuration. The calculations show that the shear band speed C is not affected when changing the value of w_{el} from 150 to 250 μm. It is also important to note that, in the adiabatic case, no critical velocity V_c is observed for the shear band propagation. Mercier and Molinari (1998) have already reported heat conduction to be responsible for the existence of this critical velocity V_c.

Then, if we introduce in the adiabatic problem an arbitrary value of w_{el} (100 μm), the results concerning the shear band velocity are quite similar to those obtained when accounting for heat conduction, excepted for $V < V_c$. Consequently, the shear band width has only a slight influence on the shear band speed (for a reasonable variation of w).

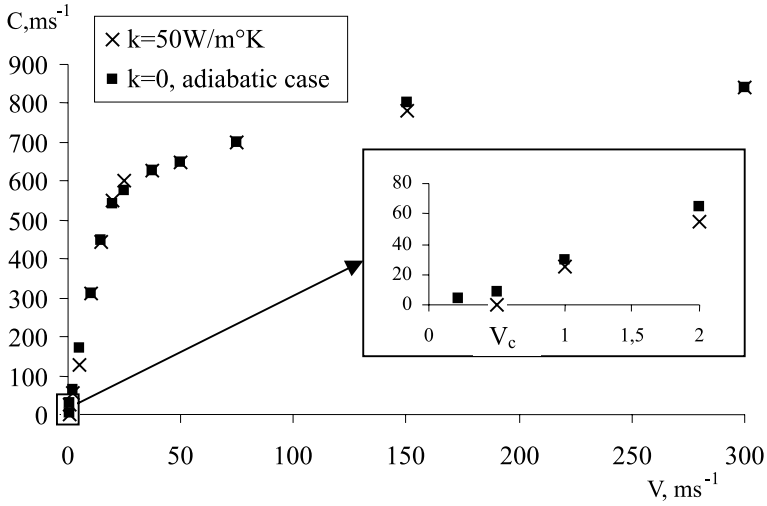

Fig. 8. Effects of the applied velocity V on the stationary shear band speed C for a CRS 1018 steel; comparison between the adiabatic case and the problem with heat conduction. In the adiabatic case, the value of the shear band width is arbitrarily controlled by the width w_{el} of the central element (at $y = 0$). Calculations are conducted by taking w_{el} equal to the width obtained in the calculations with heat conduction. V_c is the critical applied velocity beyond which the shear band propagates in the thermal conducting material. Note that $V_c = 0$ in the adiabatic case.

To summarize, the main effects of heat conductivity are the following:

- the shear band width is structured by heat diffusion,
- heat conductivity is responsible for the existence of a critical velocity V_c below which no shear band propagation is observed.

For $V > V_c$, the propagation process is quasi adiabatic and the shear band velocity is almost unaffected by heat diffusion (for instance weak effect of w on C).

3.5. Energy balance

The energy balance written for the whole volume is:

$$\dot{W} = \dot{K} + \dot{E} + D \tag{11}$$

in the adiabatic case. $\dot{W}$ is the rate of external work, $\dot{K}$ is the rate of change of kinetic energy, $\dot{E}$ is the elastic energy release rate and D is the rate of plastic deformation work. The variation of kinetic energy is due to the change of the velocity profile resulting from the propagation of the shear band tip. The change of elastic energy corresponds to the energy recovered from the stress drop behind the shear band tip.

According to the numerical results, the following observations are made:

- $\dot{K} + \dot{E} < 0$ for stage I,
- $\dot{K} + \dot{E} > 0$ for stages II and III.

The expression characterizing the transition between stages I and II is

$$\dot{K} + \dot{E} = 0 \tag{12}$$

The velocity V^* corresponding to this transition can be evaluated by giving approximative expressions for $\dot{K}$ and $\dot{E}$. The expression for $\dot{K}$ is:

$$\dot{K} = \frac{4}{3}\rho V^2 \left(h - \frac{w}{2}\right) C \tag{13}$$

The kinetic energy K has been evaluated at two times t and $t + \delta t$. During this time interval, the shear band has covered the distance $C\delta t$. The rate of change of kinetic energy $\dot{K}$ is obtained by considering a slice of length $C\delta t$ submitted to a change of velocity profile from a linear one to a piecewise constant one corresponding to rigid body motions, see Fig. 3b.

Considering τ as the value of the shear stress far ahead the tip of the band, the numerical results obtained with the constitutive law reported in (3) reveal a stress drop to the value $\tau/2$ far behind the shear band tip. Thus the rate of change of elastic energy of the specimen is:

$$\dot{E} = -\frac{3}{2}\frac{\tau^2}{\mu} hC \tag{14}$$

Using the law (7) instead of (3), the stress almost drops to zero far behind the shear band tip. The expression for $\dot{E}$ becomes:

$$\dot{E} = -2\frac{\tau^2}{\mu} hC \tag{15}$$

Using (12) with (13) and (14), V^* is evaluated as:

$$V^* = \sqrt{\frac{9\tau^{*2} h}{8\mu\rho(h - \frac{w}{2})}} \tag{16}$$

Replacing (14) by (15), V^* becomes

$$V^* = \sqrt{\frac{3\tau^{*2}h}{2\mu\rho(h-\frac{w}{2})}} \tag{17}$$

where τ^* is the shear stress far ahead the band tip, corresponding to the applied velocity V^*. The shear band width w is small with respect to the width of the shear layer $2h$. Thus V^* depends weakly upon the shear band width in general and (16) and (17) can be approximated by:

$$V^* = \sqrt{\frac{9\tau^{*2}}{8\mu\rho}} \quad \text{and} \quad V^* = \sqrt{\frac{3\tau^{*2}}{2\mu\rho}} \tag{18}$$

The relationship (18) give implicit expressions for V^*, since τ^* depends on V^*. By iterative evaluations, we obtain $19 \leqslant V^* \leqslant 22$ m/s. These values of V^* are comparable to the one provided by numerical simulations, i.e. approximately 20 m/s.

3.6. Influence of material properties on V^*

The relationship (17) clearly illustrates the influence on V^* of the elastic shear modulus, of the mass density and of the stress level. These dependencies are verified to be in agreement with the results of numerical simulations (see Table 2).

Reporting the value of V^* calculated above on the C–V diagram, see Fig. 5, it can be checked that V^* characterizes the end of the linear part of the diagram (stage I).

3.7. Dimensional analysis

A dimensional analysis is made in order to present and analyse the numerical results in a rational way. A special attention is accorded to the dependence of the shear band speed (C) with respect to the material parameters (μ: elastic shear modulus, ρ: mass density, C_p: specific heat, k: heat conductivity, n: strain hardening, m: strain rate sensitivity, β: Taylor–Quinney coefficient, K: stress level), to the loading conditions (V: applied velocity, T_0: initial temperature) and to geometry (h: half width of the sheared layer, L: length of the layer, e_{def}: defect thickness)

Using the Vashy-Buckingham theorem, the following relationship is obtained:

$$\frac{C}{V} = F\left(\frac{K}{\mu}, \frac{\rho V^2}{\mu}, \frac{\rho C_p T_0}{\mu}, \frac{kT_0}{V\mu h}, \frac{h}{L}, \frac{h}{e_{\text{def}}}, m, n, \beta\right) \tag{19}$$

Table 2
Comparison between the values of V^* calculated with (18) and those obtained by numerical simulations

Properties	V^* (m/s) calculated with (18)	V^* numerical simulations (m/s)
$\mu = 80$ GPa, $\rho = 7800$ kg m^{-3}, $K = 6300 \times 10^6$ Int. Syst.	$19 \leqslant V \leqslant 22$	≈ 20
$\mu = 40$ GPa, $\rho = 7800$ kg m^{-3}, $K = 6300 \times 10^6$ Int. Syst.	$27 \leqslant V \leqslant 31$	≈ 30
$\mu = 580$ GPa, $\rho = 7800$ kg m^{-3}, $K = 6300 \times 10^6$ Int. Syst.	$7 \leqslant V \leqslant 8$	≈ 6
$\mu = 80$ GPa, $\rho = 3900$ kg m^{-3}, $K = 6300 \times 10^6$ Int. Syst.	$25 \leqslant V \leqslant 29$	≈ 30
$\mu = 80$ GPa, $\rho = 15600$ kg m^{-3}, $K = 6300 \times 10^6$ Int. Syst.	$14 \leqslant V \leqslant 16$	≈ 12.5
$\mu = 80$ GPa, $\rho = 7800$ kg m^{-3}, $K = 9450 \times 10^6$ Int. Syst.	$27 \leqslant V \leqslant 32$	≈ 30

In the following, the function F which appears in relationship (19) is made explicit for stages I and III but is hard to be determined for the transient stage II.

3.7.1. Stage I

To determine the functional dependence (19), it is necessary to vary each non-dimensional parameter while keeping the others constant. All calculations are carried out with the constitutive law (3).

From the numerical results the following relationship is found for Eq. (19).

$$\frac{C}{V-V_c}\approx\frac{C}{V}\approx\alpha\left(\frac{K}{\mu}\right)^{0.97}\left(\frac{\mu}{\rho C_pT_0}\right)^{0.98}\beta^{1.01}\frac{1}{m^{1.08}}(-An+B) \tag{20}$$

for $V\gg V_c$. We obtain $A\approx 257$ and $B\approx 38.2$; α depends on the thermal softening exponent ν. The calculations show no influence of $\rho V^2/\mu$, $kT_0/V\mu h$, h/L and h/e_{def} on C/V. Because of the precision related to the shear band speed calculations, the exponents can be fairly approximated by 1. Thus (20) becomes

$$\frac{C}{V}=\alpha\left(\frac{K}{\mu}\right)\left(\frac{\mu}{\rho C_pT_0}\right)\frac{\beta}{m}(-An+B)=\alpha\frac{K\beta}{\rho C_pT_0m}(-An+B) \tag{21}$$

Fig. 9 shows, for instance, the evolution of the parameter C/V as a function of respectively K/μ, $\rho C_pT_0/\mu$ and n.

It is worth to emphasize that this law has been identified for a certain range of variation of the parameters beyond which no extrapolation should be made:

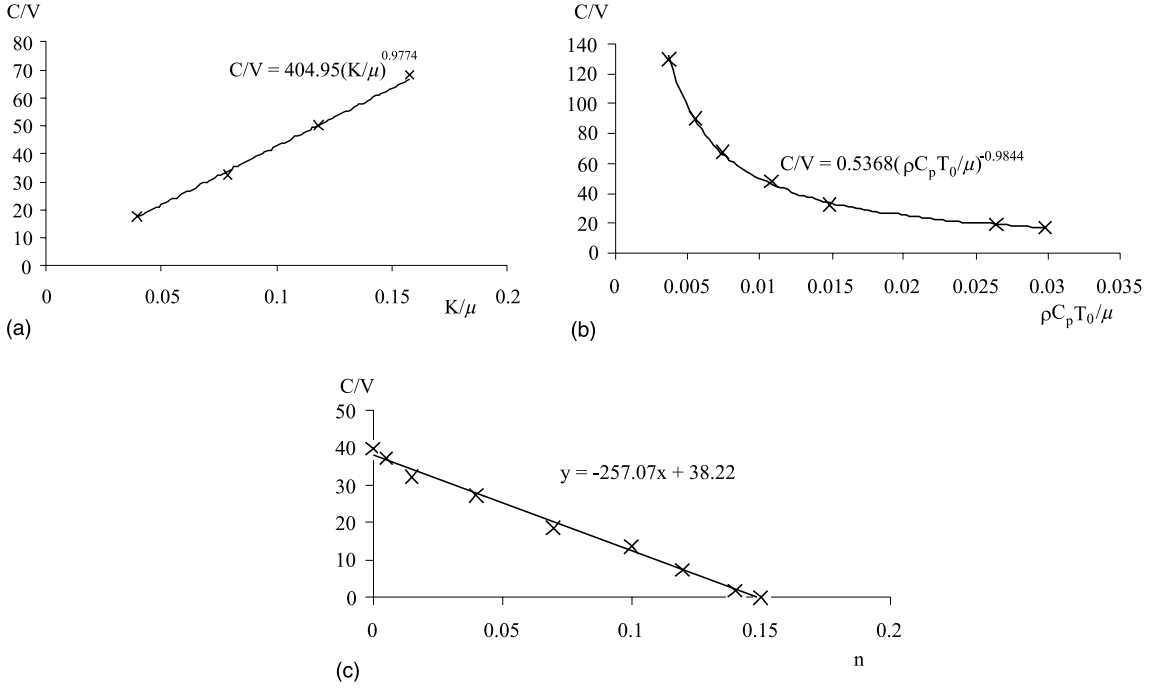

Fig. 9. Evolution of the shear band speed C normalized by the applied velocity V as a function of: (a) K/μ, (b) $\rho C_pT_0/\mu$, (c) n for fixed values of the other non-dimensional parameters. All calculations refer to stage I. The parameters involved in the problem are K/μ, $\rho V^2/\mu$, $\rho C_pT_0/\mu$, $kT_0/V\mu h$, h/L, e/e_{def}, m, n and β.

$3.15 \times 10^3 \leqslant K \leqslant 12.6 \times 10^3$ MPa,
$0.45 \leqslant \beta \leqslant 1$,
$0 \leqslant n \leqslant 0.12$,
$1950 \leqslant \rho \leqslant 15\,600$ kg m^{-3},
$125 \leqslant C_p \leqslant 1000$ J/kg K,
$75 \leqslant T_0 \leqslant 600$ K,
$0.005 \leqslant m \leqslant 0.05$,
$40 \times 10^3 \leqslant \mu \leqslant 160 \times 10^3$ MPa,
$0 \leqslant k \leqslant 500$ W/m K,
$1.25 \leqslant e/e_{\text{deff}} \leqslant 2$,
$V_c < V < V^*$

3.7.1.1. Influence of the stress level K. The increase of the shear band velocity with the flow stress level (see Fig. 9) is interpreted to be related to the higher input of external work in the system. In the vicinity of the shear band tip, K is included in two terms via the shear stress τ. The level of K affects the elastic energy $\tau^2/2\mu$ (where τ corresponds to the value of the shear stress far ahead the tip of the band) and the external rate of work τV. As C/V depends linearly on K and does not depend on μ, according to relationship (21), it can be deduced that the propagation of the shear band is controlled by the external work in stage I.

3.7.1.2. Influence of inertia effects. In the physics of the problem, inertia is likely to influence the band speed via the term ρV^2 which accounts for the kinetic energy effects. Inertia may also occur through elastic wave propagation. We postulate here that elastic shear waves are of most interest. They propagate with the velocity $C_2 = \sqrt{\mu/\rho}$. In expression (21), none of these terms appears. It can thus be deduced that the elastic wave speed does not play any role on the shear band propagation in this stage and also that the kinetic effects can be neglected for this range of velocities V ($V_c \leqslant V \leqslant V^*$).

3.7.1.3. Influence of heat generation. The term $\rho C_p T_0/\beta$ in the relationship (21) is associated to self heating due to the dissipation of the fraction β of the plastic work. From (21) it appears that an increase of C_p (or a decrease of β) leads to a diminution of the shear band speed C. Indeed, according to (8), increasing C_p (or reducing β) leads to a diminution of $\dot{T}$ for a given value of D^{p}_{eq}. As a consequence, the stress drop due to thermal softening is weaker and C decreases. Moreover, the shear band speed is dependent on the initial temperature T_0 as it controls the initial stress level according to (3): a lower initial temperature leads to an increase of the initial stress and thus to a stronger thermal softening. Consequently C increases.

3.7.1.4. Influence of the strain rate sensitivity. Increasing m has a stabilizing effect manifesting itself by a significant decrease of the shear band speed as already mentioned by Mercier and Molinari (1998). The evolution law of C/V upon m given by (21) is valid for the range of values of m considered ($0.005 \leqslant m \leqslant 0.05$). For higher values of m, shear localization cannot take place according to the instability criterion established by Molinari and Clifton (1987) for a one-dimensional process under velocity controlled boundary conditions: $m(1-v) + n + v < 0$. Note that this criterion cannot be strictly applied to the 2D problem of shear band propagation. However, it gives indications concerning the influence of material parameters on the instability process.

3.7.1.5. Influence of strain hardening. The strain hardening parameter n is also stabilizing for the shear band propagation. For $n \geqslant 0.15$, no shear band is observed (see Fig. 9).

3.7.1.6. Influence of the elastic shear modulus μ. In stage I, the dependence of C upon μ is negligible according to the relationship (21). From the physics of the problem, μ should be included through two

different terms: the elastic energy $\tau^2/2\mu$ and the elastic shear wave speed $\sqrt{\mu/\rho}$. There is no way to combine these quantities so as to eliminate μ and to be compatible with the results (21). Therefore it can be concluded that elastic energy and elastic shear wave speed have no influence on the shear band propagation in stage I. As a consequence, the fact that the external work controls the shear band propagation in stage I is confirmed.

3.7.1.7. Influence of the heat conductivity k. As shown previously there is no important effect of k on C for applied velocities in stage I excepted in the vicinity of V_c. For $V < V_c$, heat conductivity effects prevent shear band propagation.

3.7.1.8. Influence of the geometrical defect. As mentioned previously, the magnitude of the geometrical defect e_{def} has no effect on the stationary shear band speed.

3.7.1.9. Influence of the specimen length L and of the width h of the layer. The specimen length L must be high enough to allow the shear band speed to reach a stationary process, but as soon as this minimum size is attained, this geometrical parameter does not play any more role on the shear band propagation.

Moreover, the shear band velocity does not depend either on the width h of the layer, as long as h is large with respect to the shear band width w.

3.7.2. Stage III

Transient stage II is not studied in this paper, since it seems hard to get functional relationships of the type (21) or (22) for this stage. From the numerical results, the following relationship is obtained for Eq. (19):

$$\frac{C}{V} = \eta\left(\frac{K}{\mu}\right)^{0.92}\left(\frac{\mu}{\rho V^2}\right)^{0.44}\left(\frac{\mu}{\rho C_p T_0}\right)^{0.45}\left(\frac{1}{m}\right)^{0.49}\beta^{0.52}(-\mathrm{A}'n + B')$$

which is approximated by:

$$C = \eta C_2\sqrt{\frac{K^2\beta}{\mu\rho C_p T_0 m}}(-A'n + B') \tag{22}$$

where $C_2 = \sqrt{\mu/\rho}$ corresponds to the elastic shear wave speed. The values $A' \approx 34.6$ and $B' \approx 5.8$ are obtained; η depends on v. The calculations show no influence of $kT_0/V\mu h$, h/L and h/e_{def} on C/V. The evolution of the parameter C/V as a function of K/μ, $\rho V^2/\mu$, $\rho C_P T_0/\mu$ is reported in Fig. 10. The influence of parameters m, n and β is shown in Fig. 11. The analysis was driven for the following values of parameters:

$3.15 \times 10^3 \leqslant K \leqslant 12.6 \times 10^3$ MPa,
$0.3 \leqslant \beta \leqslant 1$,
$0.005 \leqslant n \leqslant 0.15$,
$3900 \leqslant \rho \leqslant 31\,200$ kg m^{-3}
$250 \leqslant C_p \leqslant 2000$ J/kg K,
$150 \leqslant T_0 \leqslant 1200$ K,
$0.01 \leqslant m \leqslant 0.12$,
$40 \times 10^3 \leqslant \mu \leqslant 160 \times 10^3$ MPa,
$0 \leqslant k \leqslant 500$ W/m K,
$1.25 \leqslant e/e_{def} \leqslant 2$,
$V > V^*$.

3.7.2.1. Influence of the stress level K. No dependence of C upon V is obtained in relationship (22) indicating that the external work does not govern the shear band propagation. Moreover, K appears through the term

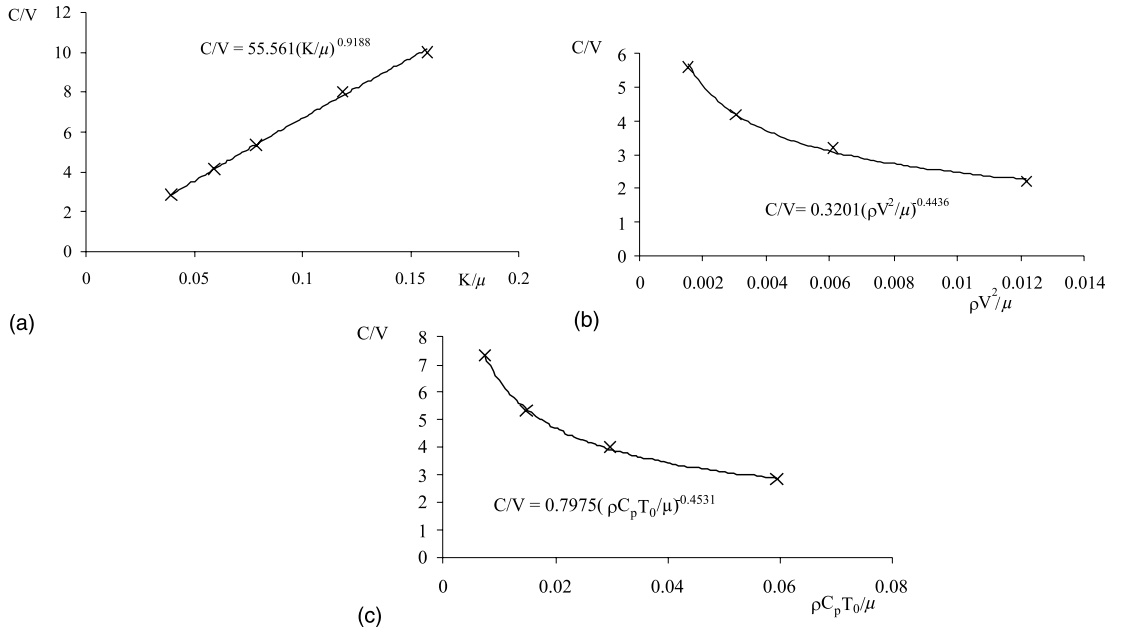

Fig. 10. Evolution of shear band speed C normalized by the applied velocity V as a function of: (a) K/μ, (b) $\rho V^2/\mu$, (c) $\rho C_p T_0/\mu$ for fixed values of the other non-dimensional parameters. All calculations refer to stage III. The parameters involved in the problem are K/μ, $\rho V^2/\mu$, $\rho C_p T_0/\mu$, $kT_0/V\mu h$, h/L, e/e_{def}, m, n and β.

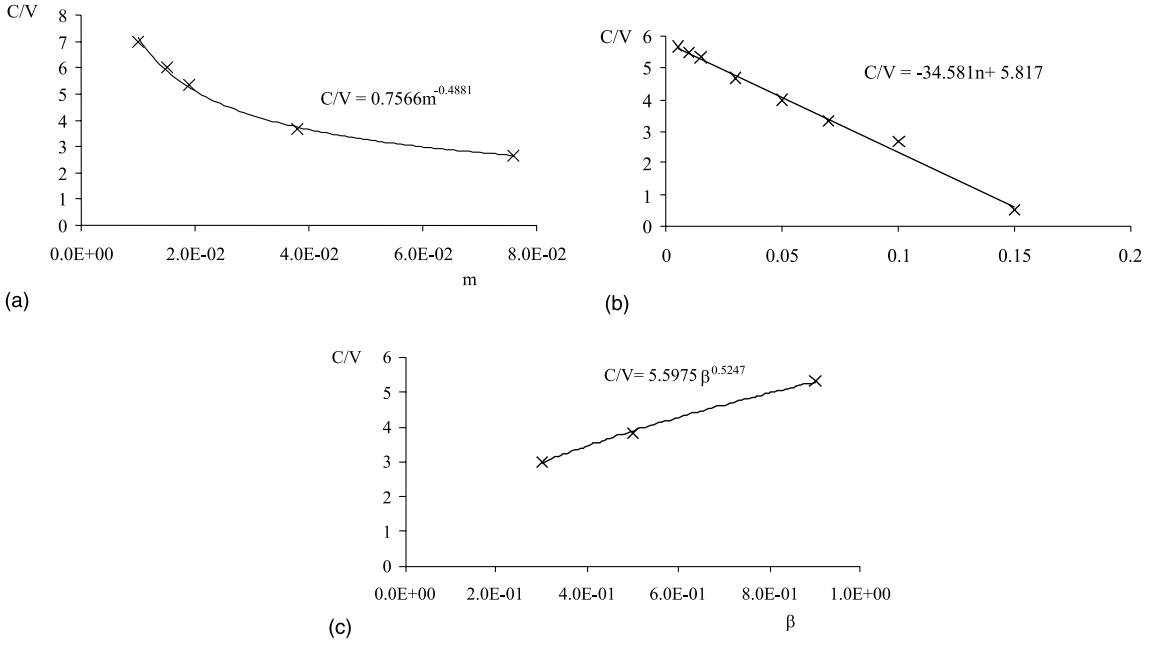

Fig. 11. Evolution of shear band speed C normalized by the applied velocity V as a function of: (a) m (b) n (c) β for fixed values of the other non-dimensional parameters. All calculations refer to stage III. The parameters involved in the problem are K/μ, $\rho V^2/\mu$, $\rho C_p T_0/\mu$, $kT_0/V\mu h$, h/L, e/e_{def}, m, n and β.

K^2/μ which scales with an elastic energy. An increase of K leads to an increase of the elastic energy release and thus to a higher shear band speed.

3.7.2.2. Influence of the elastic shear modulus μ. The elastic shear modulus is included into the elastic wave speed $\sqrt{\mu/\rho}$ and into the elastic energy term $\tau^2/2\mu$. On the one hand, as wave propagation is responsible for the elastic energy transport to the shear band tip, an increase of μ should favorize the energy flux to the band tip and should lead to an increase of C. But on the other hand, increasing μ reduces the level of the stored elastic energy in front of the band tip and should produce a decrease of C. Because of this competition between two opposite effects, a variation of μ seems to have no influence on the shear band speed.

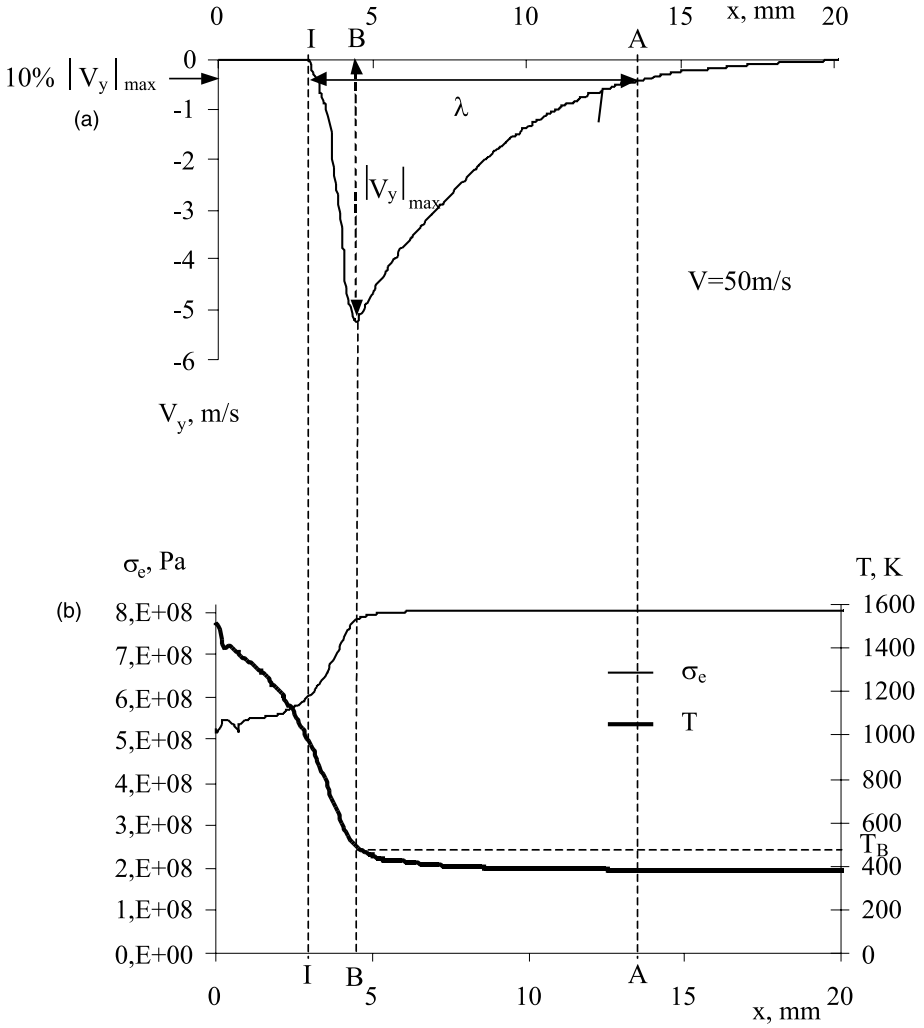

Fig. 12. (a) Definition of the characteristic size $\lambda = \mathrm{IA}$ of the process zone. The shear band tip I is defined as the point where the transverse flow vanishes ($V_y = 0$). (b) Evolution of the effective stress σ_e and of the absolute temperature T within the process zone.

3.7.2.3. Influence of inertia effects. Inertia appear in (22) through $\sqrt{\mu/\rho}$ indicating that wave propagation cannot be neglected in stage III. Reducing the elastic shear wave speed (while keeping $\mu\rho$ constant) leads to a diminution of C.

Finally, the influence of thermal effects $\rho C_p T_0/\beta$ and of parameters m, n, k, e_{def}, L and h is similar to the one characterized for stage I.

4. Process zone

To explain the physics of shear band propagation, it is important to understand the complex histories of deformation, stress and temperature experienced by material particles near the shear band tip. It is useful to introduce the concept of a process zone, which is the region at the vicinity of the shear band tip where the strain rate profile changes rapidly from a quasi-uniform to a localized distribution (see Fig. 3). Many authors have already reported that the propagation of an adiabatic shear band is determined by the critical phenomena occurring in this zone (Meyers and Kuriyama, 1986; Grady, 1992). The characteristic size (λ) of the process zone is evaluated as follows. In our configuration, the V_y component of velocity representing the flow of material from the upper to the lower part of the specimen provides a way of measuring the size of the process zone. Fig. 12a shows the evolution of V_y with respect to the position x along the line $y = 0$, for a given value of the applied velocity V (see Fig. 2 for definition of axes x and y). The shear band tip is defined as the point I where $V_y = 0$. The characteristic size of the process zone is defined as IA, with A being the point on the y-axis corresponding to 10% of the maximum value of $|V_y|$ (on the increasing branch of the curve V_y versus x).

In the Fig. 12b, the temperature and equivalent stress profiles are plotted along the line $y = 0$ for the constitutive law (3). The entrance to the process zone (at point A) is accompanied by a very slow decrease of the equivalent stress and by a small increase of temperature. A sudden stress softening and a strong temperature growth are initiated at the point B where $|V_y|$ reaches its maximum. The temperature at point B is noted T_{B}.

The stress drop at point B due to thermal softening is the motor of adiabatic shear band propagation. To illustrate this point, a comparison is made between the constitutive laws (3) and (7). Different values of the thermal softening parameter p are considered in (7). Fig. 13 shows, for the constitutive law (7) and

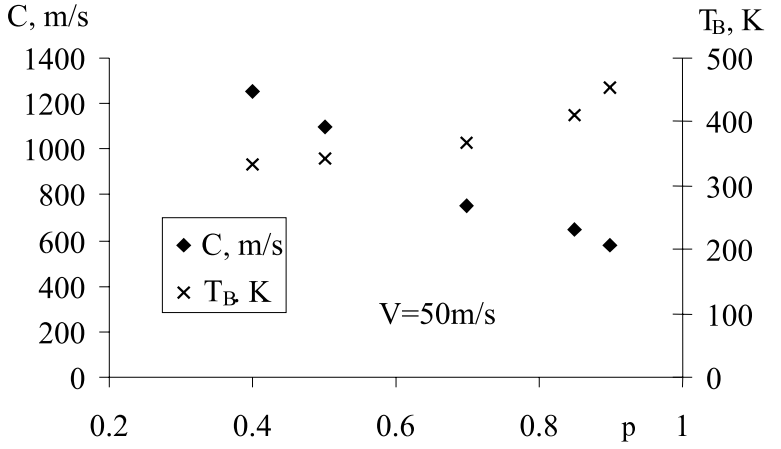

Fig. 13. Evolution of the shear band speed C and of the temperature T_{B} at point B (the core of the process zone) with respect to the thermal softening parameter p of the constitutive law (7). Small values of p correspond to a strong rate of thermal softening and to large values of the propagation speed C.

$V = 50$ m/s, the evolution of C and T_B with respect to p. Small values of p correspond to a strong rate of thermal softening and to large values of the propagation speed C. This indicates that the shear band propagation is driven by thermal softening. This is further demonstrated by the results of Fig. 14a where $\partial\sigma_e/\partial T$ is represented as a function of T for different p. The values of $\partial\sigma_e/\partial T$ at the point B (temperature T_B) are stressed with circles. Comparing with Fig. 13, it appears that the higher the values of $|\partial\sigma_e/\partial T|$ at T_B (characterizing thermal softening), the more rapidly the band propagates. The evolution of $\partial\sigma_e/\partial x$ with

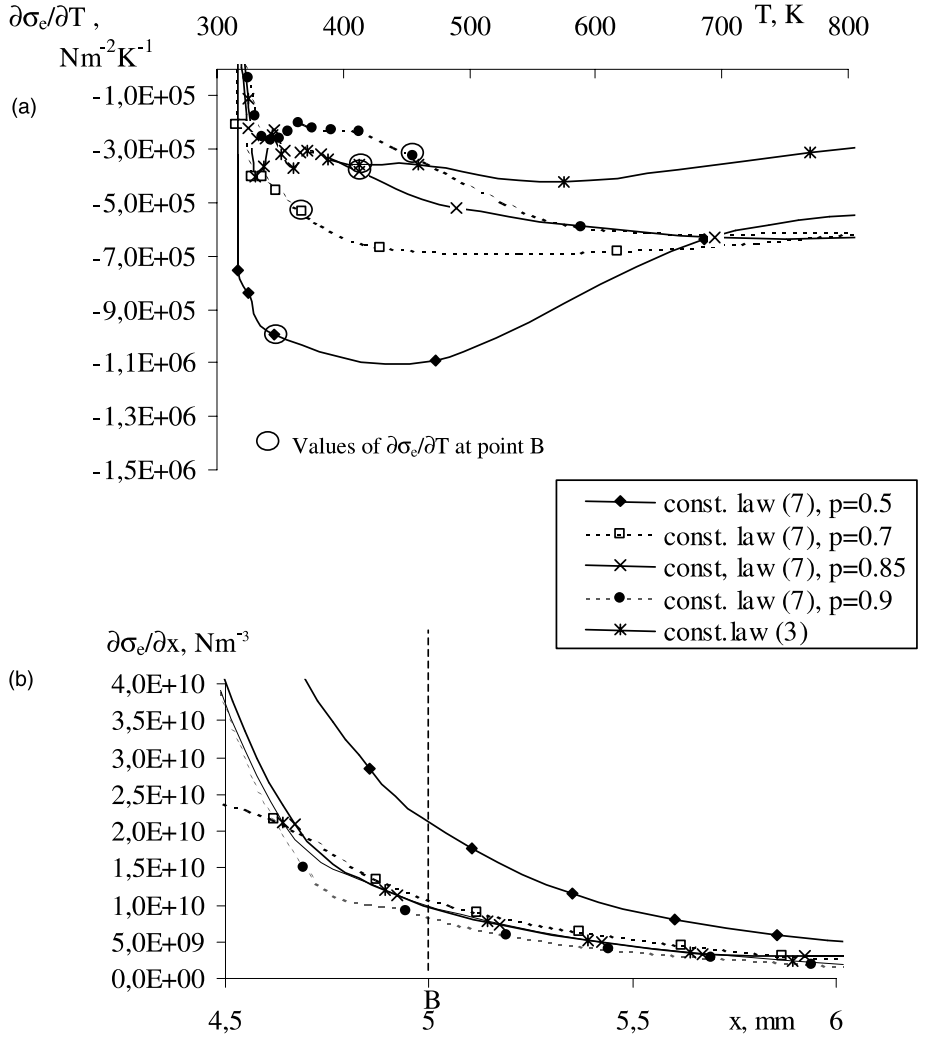

Fig. 14. (a) Evolution of $\partial\sigma_e/\partial T$ as a function of T for several values of p. Fig. (a) is obtained by elimination of the spatial variable x between $\partial\sigma_e/\partial T$ $(x, y = 0)$ and $T(x, y = 0)$ for points $(x, y = 0)$ being in the process zone. The values of $\partial\sigma_e/\partial T$ corresponding to the temperature at the core B of the process zone are stressed by small circles. Comparing with Fig. 13, it can be noted that the largest shear band velocities are obtained for the highest values of the thermal softening $|\partial\sigma_e/\partial T|$ at B. (b) Evolution of $\partial\sigma_e/\partial x$ with respect to the position x on the y-axis of the sample. For each constitutive law, the distribution of $\partial\sigma_e/\partial x$ is represented at the time when the core B of the process zone reaches the position $x = 5$ mm. The results confirm those of (a). The constitutive laws for which the stress softening $\partial\sigma_e/\partial x$ at B is the highest produce the largest shear band velocities.

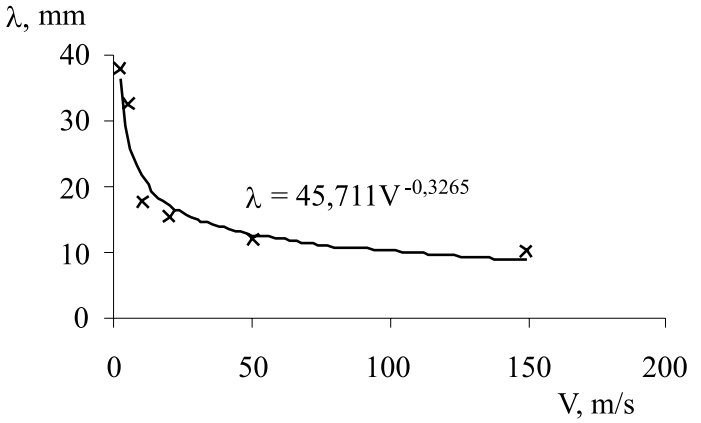

Fig. 15. Evolution of the characteristic size of the process zone λ with respect to the applied velocity V.

respect to the position x, represented in Fig. 14b confirms this remark. Indeed, the constitutive laws for which the stress softening $\partial\sigma_e/\partial x$ at B is the highest produce the largest shear band velocities.

Moreover, results for the constitutive law (3) are also reported in Fig. 14. It is reminded that for $p = 0.85$, the constitutive laws (3) and (7) coincide in the range of temperature $300 \leqslant T \leqslant 500$ K. For these two constitutive laws, the same thermal softening $\partial\sigma_e/\partial T$ is obtained within the process zone for $T \leqslant T_B$. It is remarkable, as shown in Fig. 5, that the same shear band speeds are obtained for both constitutive laws. Therefore, it is most probable that the shear band speed is controlled by the intensity of thermal softening $\partial\sigma_e/\partial T$ at the point B, which defines the core of the process zone.

Coming back to the Fig. 13, it appears that the temperature T_B increases with p. This can be explained by the fact that thermal softening is stronger for small values of p. Thus, the localization process occurs sooner and the overall temperature of the specimen is lower.

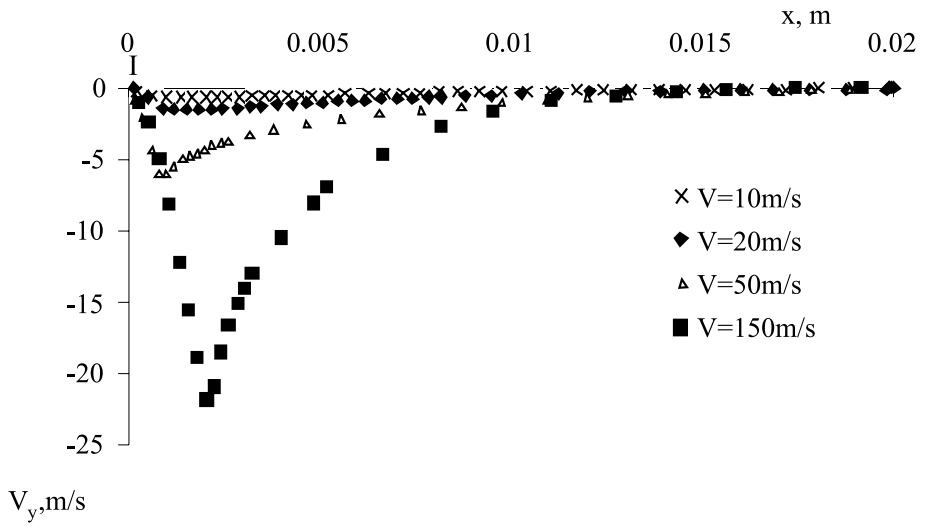

Fig. 16. Evolution of the V_y velocity component as a function of the x-coordinate on the axis $y = 0$, for several values of V. The origin of the frame is located at the shear band tip I (where $V_y = 0$). A strong dependence of V_y with V is observed.

It is also of interest to analyse the evolution of the characteristic size λ of the process zone, with respect to the applied velocity V. The results reported in Fig. 15 can be represented by the following law:

$$\lambda \approx \Phi V^{-0.32} \tag{23}$$

where Φ is a constant. The relationship (23) shows that the process zone becomes shorter when the applied velocity increases. This indicates that the flow of material from the upper to the lower part of the specimen (quantified by V_y) takes place in a shorter region. However, if we now consider the values of V_y on the line $y = 0$, it can be seen in Fig. 16 that the maximum of $|V_y|$ increases with V as:

$$|V_y|_{\max} \approx \Psi V^{1.3} \tag{24}$$

Denoting by M the volume of material which flows through the line $y = 0$ per unit of time, it can be stated that M is of the order of $\lambda|V_y|_{\max}$, which is nearly proportional to V. Mercier and Molinari (1998) have already found this dependence; more precisely they obtained the relationship $M = V(h - h_0)/2$ (where h and h_0 are the half width of the layer and the half of the shear band width, respectively).

5. Conclusion

Numerical simulations have been carried out in order to study the dynamic propagation of an adiabatic shear band in the configuration of Marchand and Duffy's experiments. A layer of finite length L and of finite width $2h$ was subjected to simple shear with constant and uniform velocities $\pm V$ applied at the upper and lower boundaries. The effect of loading conditions and of material properties on the stationary shear band speed were analysed. The influence of the applied velocity V on the shear band speed C was characterized. Three different stages were defined: the first one (stage I) which shows a strong variation of C with V, the second one (stage II) where a tendency towards an asymptotic value is seen and the last one (stage III) where C is quasi constant. An approximate value for the velocity V^* corresponding to the end of stage I was determined from an energy balance relationship.

Heat conductivity was found to be a regularizing parameter determining the width of the shear band. When the problem with heat conductivity was compared to the adiabatic case (no heat conduction), no difference was observed for the evolution of C with respect to V, excepted the fact that heat conductivity introduces a critical velocity V_c below which no shear band propagation is observed. It was also found that the shear band width has only a slight influence on the shear band speed. The velocity V_c characterizes the transition from an isothermal to an adiabatic process.

A dimensional analysis allowed to quantify the different terms governing the shear band propagation. For stage I, the dependence of C upon V is quasi-linear and the propagation is controlled by the external work provided at the specimen boundaries. In this stage, elastic wave propagation effects have a little influence as the reported shear band speeds are low. In stage III, the propagation of the shear band is controlled by the elastic energy release. Indeed, as the shear band speeds are quite high, elastic wave propagation has an important role to play in controlling the amount of elastic energy released in the vicinity of the process zone. This elastic energy is transferred and dissipated within the process zone. The value of C appears to be dependent on the elastic shear wave speed as in fracture mechanics. For each of these stages, a relationship indicating the dependence of C with respect to the loading conditions, and with respect to the material and geometrical parameters was obtained.

The shear band speed was found to be determined by the phenomena occurring inside the process zone. The size λ of the process zone decreases when the applied velocity V increases. It was demonstrated that the shear band propagation is controlled by the amount of stress softening occurring at the core of the process zone.

References

Abaqus Manuals, 2000. Version 6.1, Hibbit, Karlson and Sorensen Inc., Providence, USA.

Bai, Y.L., 1982. Thermo-plastic instability in simple shear. Journal of Mechanics and Physics of Solids 30 (4), 195–207.

Batra, R.C., Zhang, X., 1994. On the propagation of a shear band in a steel tube. ASME Journal of Engineering Materials and Technology 116, 155–161.

Clifton, R.J., 1980. Adiabatic shear banding. In: Material Response to Ultra-High Loading Rates, NMAB-365. National Materials Advisory Board (NRC), Washington DC.

Clifton, R.J., Duffy, J., Hartley, K.A., Shawki, T.G., 1984. On critical conditions for shear band formation at high strain rates. Scripta Metal. 18, 443–448.

Dinzart, F., Molinari, A., 1998. Structure of adiabatic shear bands in thermo-viscoplastic materials. European Journal of Mechanics and Solids 17, 923–938.

Gioia, G., Ortiz, M., 1996. The two-dimensional structure of dynamic shear bands in thermoviscoplastic solids. Journal of Mechanics and Physics of Solids 44, 251–292.

Giovanola, J.H., 1988a. Adiabatic shear banding under pure shear loading. Part I: direct observation of strain localization and energy dissipation measurements. Mechanics of Materials 7, 59–71.

Giovanola, J.H., 1988b. Adiabatic shear banding under pure shear loading. Part II: fractographic and metallographic observations. Mechanics of Materials 7, 73–87.

Glimm, J., Plohr, B.J., Sharp, D.H., 1993. A conservative formulation for large-deformation plasticity. Applied Mechanics Review 46, 519–526.

Grady, D., 1992. Properties of an adiabatic shear band process zone. Journal of Mechanics and Physics of Solids 40 (6), 1197–1215.

Kalthoff, J., Wrinkler, S., 1987. Failure mode transition at high strain rates of shear loading. In: Chiem, C., Kunze, H., Meyers, L. (Eds.), Impact Loading and Dynamic Behaviour of Materials, vol. 1. Informationgesellschaft Verlag Bremen, pp. 185–195.

Marchand, A., Duffy, J., 1988. An experimental study of the formation process of adiabatic shear band in a structural steel. Journal of Mechanics and Physics of Solids 36, 251–283.

Mercier, S., Molinari, A., 1998. Steady-state shear band propagation under dynamic conditions. Journal of Mechanics and Physics of Solids 46 (8), 1463–1495.

Merzer, A.M., 1982. Modelling of adiabatic shear band development from small imperfections. Journal of Mechanics and Physics of Solids 30 (5), 323–328.

Meyers, M.A., Kuriyama, S., 1986. Numerical Modeling of the propagation of an adiabatic shear band Metallurgical Transactions, 17 A, 433–450.

Molinari, A., 1988. Shear band analysis. In: Nonlinear Phenomena in Materials Science. In: Solid State Phenomena, vol. 3, Trans. Tech. Publ. pp. 447–468.

Molinari, A., Clifton, R.J., 1987. Analytical characterization of shear localization in thermoviscoplastic materials. ASME Journal of Applied Mechanics 54, 806–812.

Wright, T.W., Batra, R.C., 1985. The initiation and growth of adiabatic shear bands. International Journal of Plasticity 1, 205–212.

Wright, T.W., Ockendon, H., 1992. A model for fully formed shear bands. Journal of Mechanics and Physics of Solids 40 (6), 1217–1226.

Wright, T.W., Ravichandran G, 1997. Canonical aspects of adiabatic shear bands. International Journal of Plasticity 13 (4), 309–325.

Wright, T.W., Walter, J.W., 1987. On stress collapse in adiabatic shear bands. Journal of Mechanics and Physics of Solids 35, 701–720.

Zhou, M., Ravichandran, G., Rosakis, A.J., 1996a. Dynamically propagating shear band in impact-loaded prenotched plates II—Numerical simulations. Journal of Mechanics and Physics of Solids 44, 1007–1032.

Zhou, M., Rosakis, A.J., Ravichandran, G., 1996b. Dynamically propagating shear band in impact-loaded prenotched plates I—Experimental investigations of temperature signatures and propagation speed. Journal of Mechanics and Physics of Solids 44, 981–1006.